CLM - P 484

UKAEA RESEARCH GROUP

Preprint

EVOLUTION OF THE REVERSED FIELD PINCH

J P CHRISTIANSEN
K V ROBERTS

CULHAM LABORATORY
Abingdon Oxfordshire

1977

CLM-P484

EVOLUTION OF THE REVERSED FIELD PINCH

J P Christiansen and K V Roberts

Culham Laboratory, Abingdon, Oxon. OX14 3DB, U.K.
(Euratom/UKAEA Fusion Association)

ABSTRACT

This paper discusses the time evolution of a slow Reversed Field Pinch during the sustainment phase, starting from an initial low-β configuration at the end of the setting-up phase which corresponds approximately to a Taylor Reversed-Field Bessel-function state. Calculations are made with a 1DMHD equilibrium and diffusion code. Because of local overheating and consequent rise of plasma pressure the central region of low shear becomes Suydam unstable, and it is assumed that this results in local MHD turbulence, so flattening out the central density and temperature profiles and leading to a quasi-steady state which gradually evolves in time. The pinch then consists of two main zones, a central Suydam unstable core I and an outer MHD stable layer II which is responsible for confinement. An external Zone III may exist near the wall but is not studied here. The configuration time τ_c depends on the time for which the trapped positive B_z flux ψ_+ can persist against resistive diffusion. This in turn depends on the electron temperature in Zone II and hence on the anomalous electron thermal conductivity that is assumed in the model. Some information can be obtained by normalizing the phenomenological transport coefficients used in the code to the measurements made on ZETA but this does not provide a very sensitive check. Further information can be obtained from empirical Tokamak scaling laws. We then predict the performance of the proposed device RFX. A significant difference between ZETA and RFX is that in ZETA it was the disappearance of the negative flux ψ_- that terminated the quiescent period, while in RFX it is the positive flux ψ_+ that controls the configuration time. This leads to a substantial improvement in predicted performance.

(Submitted for publication in Nuclear Fusion)

March 1977
agc

1. INTRODUCTION

The Reversed Field Pinch (RFP) may have some advantage over the Tokamak as an economic reactor because of the higher ratio β between plasma and magnetic pressure [1]. An understanding of the performance of the RFP and how it compares with the Tokamak is therefore significant for progress in reactor design, and this paper is intended to contribute towards such an understanding by developing a theoretical and computational model for the evolution of the RFP discharge based on the available experimental evidence.

The magnetic configuration of the RFP is illustrated in Fig.1. It differs from the Tokamak in having a toroidal field B_ϕ which is comparable with the poloidal field B_θ and therefore operates well above the Kruskal-Shafranov limit. MHD instability is avoided by reversing the B_ϕ field in the outer region of the plasma so that a pitch minimum does not occur [2,3]. The lower toroidal field enables both the total β and the shear to be substantially higher than in Tokamaks.

Unlike the stellarator which can in principle operate in a steady state, and the Tokamak which can under suitable conditions maintain the discharge for as long as the volt-seconds are able to sustain the toroidal current I_ϕ, the lifetime τ_c of the RFP configuration is determined by the decay of the trapped positive B_ϕ flux which is indicated by ψ_+ in Fig.1. Once the field reversal point a_R has moved inwards from the wall, there is no way in which ordinary diffusion processes in azimuthally symmetric geometry can allow ψ_+ to increase in value, and it must inevitably decay due to the finite resistivity of the plasma. Although it might be possible to maintain or increase ψ_+ by neutral beam injection or by MHD turbulence we do not deal with such processes in this paper, and therefore consider two separate phases of the discharge:

A. The "Setting-up Phase" in which the magnetic field configuration of the type shown in Fig.1 is established by some appropriate means.

B. The "Sustainment Phase" in which the B_ϕ configuration gradually relaxes to the point at which stable confinement of a hot high-β plasma can no longer be maintained.

Phase A is complicated in both the Tokamak and the RFP and probably involves MHD instabilities or turbulence. We shall not attempt to follow it in this paper although some discussion is given. Our main purpose is to develop a model for the evolution of slow reversed field pinches during the sustainment phase B based on 1DMHD computer calculations similar to those for Tokamaks [4].

The model envisages that in phase B the RFP discharge should consist of three main concentric zones as indicated in Fig.2. The central Zone I of radius a_1 (where a_1 can be 10 - 50% of the minor radius a) is expected to be MHD turbulent at a rather low level caused by Joule overheating, which raises the plasma pressure in a region of very weak shear and so leads to Suydam instabilities. These instabilities should in turn lead to enhanced diffusion of plasma and energy thus flattening out the profiles and maintaining an approximate balance. It is interesting that both Tokamaks [5,6,7] and stellarators [8] also appear to have central unstable zones although these are observed to undergo periodic saw-tooth oscillations rather than random turbulence.

Zone II of radius a_2 is a region of high shear which is expected to provide stable MHD confinement. A crucial element in our argument is that the Suydam instabilities which are localized in Zone I should not lead to anomalous effects in Zone II, but only to small-amplitude Lagrangian fluctuations of the magnetic surfaces which preserve their topology and therefore do not allow the plasma to diffuse across the magnetic field. This question is discussed further in section 5. Zone III is an outer region in which wall interactions are expected to be important, but little is known about this zone in RFP geometry as yet and it is not dealt with explicitly in this paper.

The decay of the trapped positive B_ϕ flux ψ_+ is determined mainly by the parallel resistivity $\eta_{\parallel}$, and experiments on many types of device indicate that this is likely to be classical apart from a factor Z_{eff} of order $1 \lesssim Z_{eff} \lesssim 10$. The main uncertainty affecting $\eta_{\parallel}$ and therefore the configuration time τ_c is expected to be the electron temperature profile, and this depends quite critically on the electron thermal conductivity that is assumed for Zone II. Little empirical information is available on electron energy confinement in RFP geometry, and therefore calculations have been made for several values of the electron thermal conductivity ranging from purely classical to the level of anomaly that is observed for Tokamaks [9,10].

The main evidence for millisecond containment of high-β plasma in RFP geometry is provided by ZETA [11,12]. Reversed-field configurations were not programmed directly in ZETA, which was surrounded by a B_ϕ-flux conserving shell so that

$$\psi \equiv \psi_+ - \psi_- = \text{constant} \quad ,$$

but they were observed to occur spontaneously for certain ranges of toroidal current I_ϕ and B_ϕ flux, so leading to a "quiescent period" of enhanced stability which lasted until ψ_- had decayed to zero by resistive diffusion. Subsequent theoretical predictions by Taylor [13] and more recently by Kadomtsev [14] suggest that a force-free RFP configuration should develop spontaneously during the unstable setting-up phase A as the plasma tries to relax towards a minimum energy state, and although the details of the formation of the RFP in this way are not yet understood these theories do help to explain why it should occur. Another method to generate an RFP is by fast programming of the currents in the external coils as is done on HBTXI at Culham [15].

Large RFP devices such as ZETA (a = 0.5 m) and small fast devices such as HBTXI (a = 0.06 m) appear to operate in different regimes, due to a considerable difference in the ratio of the Alfvén or MHD instability growth

time τ_A to the current rise time τ_R and the configuration time τ_c in the two cases. In fact $\tau_A \propto N^{\frac{1}{2}}/B$ is roughly independent of radius a and of order 10 microseconds in most pinch devices, where N is the line density and B is the magnetic field, while τ_R and τ_c both increase with a. In order to predict the performance of future large devices it is therefore natural to start from the experimental results obtained on ZETA in which both phases A and B occupied a period equivalent to many instability growth times, so leading to a quasi-stationary level of turbulence [16] rather than to a single non-linear unstable mode as in HBTXI [15].

The available ZETA results [11,12] include measurements made to determine the initial structure of the RFP configuration formed during the setting-up phase A as well as measurements of the discharge behaviour during the subsequent "quiescent period" (current sustainment phase B). The approach adopted in this paper is to regard these measurements as an empirical reference point on which studies of the RFP will be based. We discuss results obtained from computer calculations with a 1D MHD model to be described in the following section. The model includes a number of physical effects which are believed to affect the behaviour of ZETA, and adjustments are made until an acceptable measure of agreement between experiment and calculation is established. Account is also taken of empirical scaling laws based on Tokamak performance [9,10].

Having normalized the model in this way, we then present results from an extensive series of calculations that aim at predicting the performance of a proposed "next generation" RFP device (a = 0.6 m) referred to as RFX (Reversed Field Experiment), whose main parameters are given in section 8. An important practical difference from ZETA is that RFX is designed to support the reversed flux ψ_- by slow programming of the B_ϕ field at the wall, so that whereas in ZETA the stable quiescent period lasted until the negative flux ψ_- had decayed away, in RFX it is the decay of trapped positive flux ψ_+ that is important. Since the positive flux occupies a

region of the discharge which is hotter, of greater radial thickness and less subject to interference from impurities or poor magnetic field geometry near the wall, one would expect that such a facility should bring about a substantial improvement in performance over that of ZETA. This is indeed one of the main results of our work.

The paper is arranged as follows. The MHD equations which are to be solved numerically are given in section 2. To see that anomalous transport and heating processes must be included we highlight in section 3 the containment features of the RFP by examining the force-free model considered in [13]. It is realized that an ohmically heated RFP configuration is likely to violate the Suydam criterion [2,3] necessary for stability, in the central regions of the discharge. We therefore need to study instabilities that may arise from "overheating" which causes a rise in pressure and to estimate their effects. Section 4 contains results from ideal MHD-stability theory and these are supplemented by 1D stability calculations which employ the numerical methods described in references [17,18]. The instabilities caused by over-heating of the central RFP region are expected (section 5) to lead to turbulent transport processes as previously suggested in [3].

The experimental data and numerical parameters used for the calculations on ZETA are given in section 7 together with the calculated results. The agreement between experiment and theory turns out to be relatively insensitive to assumptions about anomalous electron energy transport in the confining layer mainly because the temperature did not greatly exceed 100 eV. The predicted performance figures for the RFX which are presented in section 8 do on the other hand depend upon the behaviour of the confining layer since in this new device the temperature is expected to be considerably higher. Thus to bracket our predictions we have investigated what happens as the electron energy confinement properties of the outer layer are altered, and we have related our assumptions to empirical Tokamak data [9,10]. The

uncertainty surrounding this procedure is discussed in the last section.

SI units are used throughout the paper with temperatures quoted in eV.

2. SUMMARY OF THE PHYSICS MODEL

A one-dimensional cylindrical approximation is used with coordinates (r,θ,z) and functions depending only on r. In the following z will denote the toroidal coordinate ϕ used in the Introduction, so that the components of the magnetic field are B_θ (poloidal or azimuthal) and B_z (toroidal or axial). The plasma is described by an electron density n, ion and electron temperatures T_i and T_e, and effective values Z_{eff}, A_{eff} of the charge and atomic numbers. It is assumed to evolve through a sequence of states in pressure equilibrium with the field

$$\underline{\nabla} p = \underline{J} \times \underline{B} \quad , \tag{1}$$

where the pressure is $p = nk(T_e + T_i/Z_{eff})$ and the current density is given by $\mu_o \underline{J} = \underline{\nabla} \times \underline{B}$. Each new equilibrium state (1) is reached after diffusion of the magnetic field and the plasma temperatures:

$$\frac{\partial \underline{B}}{\partial t} - \underline{\nabla} \times \underline{v} \times \underline{B} = \frac{-1}{\mu_o} \underline{\nabla} \times (\underline{\underline{\eta}} \cdot \underline{\nabla} \times \underline{B}) \tag{2}$$

$$\frac{nk}{\gamma - 1} \frac{DT_e}{Dt} = - \underline{\nabla} \cdot \underline{F}_e - K + Q_e \tag{3}$$

$$\frac{1}{Z_{eff}} \frac{nk}{\gamma - 1} \frac{DT_i}{Dt} = - \underline{\nabla} \cdot \underline{F}_i + K + Q_i \quad , \tag{4}$$

where $\frac{D}{Dt}$ denotes a Lagrangian derivative. The anisotropic resistivity tensor $\underline{\underline{\eta}}$ contains contributions $\eta_{\parallel}$, $\eta_{\perp}$ from the scalar resistivities parallel and perpendicular to $\underline{B}$. The thermal fluxes $\underline{F}_e$, $\underline{F}_i$ across the field have the form $\kappa_{\perp} \frac{\partial T}{\partial r}$. K denotes the classical energy exchange rate and the source terms Q_e, Q_i include ohmic heating, Bremsstrahlung and turbulent ion heating. No plasma is lost at the confining wall r = a, but energy is lost at the

rate

$$-\left(\kappa_{\perp}\frac{\partial T}{\partial r}\right)_{r=a} .$$

The transport coefficients are expressed in the calculations in the form

$$\eta_{\parallel} = \eta_{\parallel}^{o} , \tag{5}$$

$$\eta_{\perp} = \eta_{\perp}^{o} + 4\beta\mu_{o} D_{T}' \tag{6}$$

$$\kappa_{\perp e} = \kappa_{\perp e}^{o} + nk\,(D_{T}'' + D_{a}) , \tag{7}$$

$$\kappa_{\perp i} = \kappa_{\perp i}^{o} + (n/Z_{eff})kD_{T}''' , \tag{8}$$

where superscript ^{o} denotes the classical value, and the anomalous diffusion coefficients D_T and D_a are discussed in sections 5 and 6. Energy conservation is ensured [19] by including turbulent heating contributions proportional to D_T in the ion and electron source terms.

We shall also frequently refer to a set of parameters which are commonly employed to characterize an RFP configuration. These are defined as follows:

Axial Beta $$\beta_{o} = \frac{2\,\mu_{o}\,p(o)}{B_{z}^{2}(o)} \tag{9}$$

Poloidal Beta $$\beta_{\theta} = \frac{(4\pi)^{2}}{\mu_{o}\,I_{z}^{2}} \int_{o}^{a} p\,r\,dr \tag{10}$$

Pinch parameter $$\Theta = \frac{B_{\theta}(a)}{\langle B_{z}\rangle} \tag{11}$$

Field reversal ratio $$F = \frac{B_{z}(a)}{\langle B_{z}\rangle} \tag{12}$$

Pitch function $$P(r) = \frac{r\,B_{z}(r)}{B_{\theta}(r)} . \tag{13}$$

The calculations described in sections 7 and 8 have been performed with a computer code [20] which solves equations (1) - (4) in finite difference form.

3. RFP CONTAINMENT

A qualitative picture of the evolution of the RFP is obtained by starting at the beginning of Phase B from the force-free ($\beta = 0$) Bessel function model studied in [13]. The unperturbed field components are given by the Bessel functions

$$B_z = B_o J_o(2\Theta \frac{r}{a}) \quad , \quad B_\theta = B_o J_1 (2\Theta \frac{r}{a}) \tag{14}$$

where B_o is the magnetic field on axis, and the current density has the components

$$J_z = \frac{2\Theta}{\mu_o a} B_z \quad , \quad J_\theta = \frac{2\Theta}{\mu_o a} B_\theta \ .$$

Fig.3(a) shows the components of $\underline{B}$ and $\underline{J}$ as a function of wall radius or Θ, and for $\Theta \lesssim \Theta_I = 1.587$ this configuration is stable according to ideal MHD theory [21,22]. To eliminate resistive instabilities [23,24] (tearing modes) the radius a of the conducting wall must be moved inwards relative to the field configuration so that $\Theta \lesssim \Theta_T = 1.552$ [25]. Fig.3(a) shows the two wall positions Θ_I and Θ_T. It cannot however be brought in beyond the field reversal point $\Theta_R = 1.202$, since although the configuration would still be theoretically stable with the boundary conditions appropriate to plasma in electrical contact with a perfectly conducting wall, the more realistic boundary condition of a thin vacuum layer between the plasma and the wall would lead to a point of zero shear and therefore to ideal MHD instability.

We now imagine that plasma pressure ($\beta > 0$) is added to the configuration (14), "inflating" it in such a way that magnetic flux is conserved. During this process it undergoes a Lagrangian distortion. The maximum Suydam stable value $\beta_o \equiv \beta(r = 0)$ that can be obtained on axis is calculated by inward integration of the marginally stable pressure gradient [3,21]

$$\nabla p_S = - \frac{r}{8\mu_o} B_z^2 \left(\frac{1}{P} \nabla P\right)^2 \ , \tag{15}$$

starting from the boundary condition $p_S\,(a) = 0$ and allowing for pressure

equilibrium. In Fig.3(b) the maximum values of β_o for various wall radii (or Θ) are represented by the curve labelled β_S. The curve to the right in Fig.3(b) labelled Θ_I calculated by Robinson [26] shows as a function of β_o the maximum value of Θ at which the pressure-inflated Bessel-function configuration is marginally stable against ideal MHD gross kink modes. If resistive effects are taken into account then stability against tearing modes [26,27,28] requires $\Theta \lesssim \Theta_T < \Theta_I$ with $\Theta_I - \Theta_T$ of the order of a few percent [27].

Our basic model will be that the setting-up phase A produces an initial Bessel-function field distribution with $1.2 < \Theta < 1.6$ following the prediction by Taylor [13], with plasma of finite density and negligible temperature. According to Newton [29] this initial configuration can be thought of as an "empty, elastic magnetic bottle". During the current sustainment phase B the empty bottle is gradually filled and inflated as the temperature is raised by ohmic heating, so increasing the axial value β_o. The maximum value of β_o which can be reached is indicated by the curve β_S in Fig.3(b), and the distinctive bowl shape of this curve emphasizes the need for high shear ($\Theta > 1.5$) if high values of β ($\beta > 0.1$) are to be achieved.

Writing equation (11) as

$$\Theta = \frac{a\,\mu_o}{2}\,\frac{I_z}{\psi_+ - \psi_-}$$

(where I_z is the total current, and ψ_+ and ψ_- are the positive and negative B_z fluxes) we see that the maximum β_o that can be supported in a Suydam stable state depends on the choice of total current and B_z flux. Once the RFP has been set up a further increase of Θ (and thus of β_o) is in principle possible by controlling the total current I_z via the electric field E_z at the wall, and/or by controlling the negative flux ψ_- in the outer region via the electric field E_θ at the wall. The control of wall fields (as in RFX, but not in ZETA) might thus result in very high values of β_o, so

it is therefore necessary to ask what actually happens when a low β RFP configuration evolves through the current sustainment phase B: that is, which of the stable high-β configurations can be reached and maintained during the evolution of the plasma.

The function $|\underline{J}|^2$ which is a measure of the ohmic heating rate is shown in Fig.4 together with the pitch profile corresponding to (14). It is clear from these two curves that the heating rate is at maximum where the shear $\sim \nabla P$ is at a minimum so that we should expect the Suydam stability criterion

$$\nabla p > \nabla p_S \tag{16}$$

to be violated quite quickly in the central region of the RFP. Violation of (16) will result in instabilities whose growth rates and radial eigenfunctions according to linear MHD stability theory depend on the pressure equilibrium as well as on the extent to which (16) is violated. It is not well understood how an instability grows into the non-linear regime and what happens subsequently. Using intuitive arguments based on linear stability theory, we therefore develop in sections 4 and 5 a model in which local violation of (16) leads to a local "turbulent" transport of plasma and energy across the magnetic field. Within any Suydam-unstable zone this turbulent transport will tend to flatten the density and temperature profiles so that the departure from marginal stability is automatically reduced. A related "marginal stability" approach to the enhanced transport resulting from other types of instability has been pursued by Manheimer et al [30]. Within a Suydam-stable zone we postulate that the MHD confinement properties remain intact, although the transport across such a zone will be enhanced by a steepening of the gradients to balance the flattening elsewhere, and anomalous transport due to microinstabilities may also be present. The steepening of the gradients may become sufficient to violate (16) so causing the inter-zone boundary to move.

A model of this kind was proposed by Suydam [3] in his 1958 Geneva

Conference paper ($\mu = \frac{1}{P}$) :

> "The result seems to go qualitatively as follows: the mixing of a small unstable region leads to a distribution which is less unstable on the inside and more unstable on the outside. Thus, if some interior shell were unstable, it would mix until stable, and this in turn would upset the stability of the next shell which would proceed to mix and so on. In this fashion such an instability would eat its way outward towards the surface. If, however, a layer near the surface is given excess stability, the outward progression of the mixing should be stopped. This excess stability of the surface layers ought to be insured if the B_z field were so programmed that μ' is made quite large in this region. The simplest programming appears to be one which would reverse B_z in the vacuum after the plasma has pinched."

Sakanaka and Goedbloed [31] also concluded from their study of Suydam unstable modes that these if sufficiently localized "would possibly result in enhanced diffusion"; non-localized unstable modes would "lead to the usual kink-like loss of plasma". The measurements by Robinson and Rusbridge [16] of the density fluctuations in ZETA suggest a "central core region in which the turbulence is approximately homogeneous".

This proposed distinction between "turbulent" and "confining" zones is analogous to the situation in many stars [32], but requires justification in the MHD case.

4. LOCALIZED MHD INSTABILITIES

The stability of diffuse pinch configurations has been studied extensively and references [2,3,21-26,31,33-39] represent only a small cross section of the papers published in this area. In ideal MHD theory the departure from pressure equilibrium

$$\underline{\nabla} p = \underline{J} \times \underline{B} \tag{17}$$

is described by a Lagrangian displacement vector $\underline{\xi}$, which in cylindrical geometry is represented by

$$\underline{\xi} = \sum_{m\,k} \underline{\xi}_{mk}\, e^{i(m\theta+kz-\omega t)} \quad , \quad \underline{\xi}_{mk} = (\xi, \xi_\theta, \xi_z)$$

where we have dropped the subscript from the r-component for brevity. In

the linear regime each eigenmode $\underline{\xi} = \underline{\xi}_{mk}$ satisfies an equation of motion

$$- \rho\omega^2 \underline{\xi} = \underline{F} \{\underline{\xi}\} \tag{18}$$

where ρ is the mass density and the force operator is given in [34]. The complicated form of $\underline{F}$ makes it impracticable to solve this equation analytically for arbitrary profiles of p and $\underline{B}$. Unless certain approximations are made (low shear, localization etc.) as in references [31,33-37] equation (18) has therefore to be solved numerically.

The case of marginal stability ($\omega^2 = 0$) is algebraically more straightforward and many authors have therefore approached the MHD stability problem by examining the change in energy [21]

$$\Delta W = - \frac{1}{2} \underline{F} \{\underline{\xi}\} \cdot \underline{\xi}$$

caused by a displacement $\underline{\xi}$. The equilibrium (17) is unstable if a displacement exists for which $\Delta W < 0$. Minimization of ΔW leads to the familiar expression [21]

$$\Delta W = \int_0^a \left(f \left(\frac{\partial \xi}{\partial r} \right)^2 + g \, \xi^2 \right) dr \quad , \tag{19}$$

the minimizing eigenfunctions ξ being the solutions of the Euler-Lagrange equation

$$\frac{\partial}{\partial r} f \frac{\partial \xi}{\partial r} - g \, \xi = 0 \quad . \tag{20}$$

The functions f and g as given in [21] are

$$f = \frac{1}{\mu_o} r \frac{F^2}{K^2} \tag{21}$$

$$g = \frac{2k^2}{K^2} \nabla p + \frac{2k^2}{\mu_o} \frac{FF^*}{rK^4} + \frac{1}{\mu_o} r F^2 \left(1 - \frac{1}{r^2 K^2} \right) \quad , \tag{22}$$

where

$$F = \underline{K} \cdot \underline{B} = k B_z + \frac{m}{r} B_\theta$$

$$F^* = \underline{K}^* \cdot \underline{B} = k B_z - \frac{m}{r} B_\theta$$

$$K^2 = k^2 + \frac{m^2}{r^2} \quad .$$

The Euler-Lagrange equation (20) has a singularity when f = 0, i.e. at any radial point r_s where

$$F \equiv kr_s B_z + mB_\theta = 0$$

or

$$P(r_s) = - m/k \qquad (23)$$

where P is the pitch. In the case of a monotonically decreasing RFP pitch profile similar to that of Fig.4, we see that for given m, there will be one such point r_s at which (23) is satisfied for any k in the range

$$- mP(o) < k < mP(a) \quad .$$

The eigenvalue equation that determines the frequency of modes with $\omega^2 \neq 0$ has a structure similar to that of (20) but with coefficients $f(\omega^2)$, $g(\omega^2)$ that are frequency-dependent [38]. For unstable modes ($\omega^2 < 0$, $\gamma = - i\omega$) the coefficient f is everywhere positive and the equation (20) is non-singular, but the modes of interest in this paper are mainly those whose eigenfunctions are localized near the point r_s defined by (23).

Since the first term in (19) is non-negative it is necessary for stability that g < 0 in some region between r = 0 and r = a. This can be caused either by the first or second term in (22), or both, and will give rise to various types of modes [33]. The distinction between these types of modes is most easily established for low shear systems, (see for example the discussions in [34,35] based on the equation of motion (18)). If the energy driving an instability is dominated by the second term of (22) the mode is called a kink ($\nabla p = 0$) or quasi-kink ($\nabla p \neq 0$), both modes being driven by the current. If the energy is dominated by the first term in (22) we have a pressure-driven mode, and for a configuration of zero or low shear there is a transition as ∇p is increased from quasi-interchange modes which are present only when $F \neq 0$, to pure interchange modes which are present for both F = 0 and $F \neq 0$, but are dominant at F = 0.

In the following we shall look at pressure-driven modes in a high-shear

system (the RFP) and allow for large pressure gradients. The most dangerous radius is r_s where the first term in (19) vanishes. Using the variable $x = r - r_s$ to expand around this point we see that f is quadratic in x (equation 21), while the three terms in g (equation 22) are respectively constant, linear and quadratic in x. Near the singularity the second and third terms in g may be neglected and the solutions of the Euler-Lagrange equation are [21]

$$\xi \sim x^{\nu} \quad , \quad \nu = -\frac{1}{2} \pm \frac{1}{2} (-\Sigma)^{\frac{1}{2}} \tag{24}$$

where the parameter Σ which measures the departure from a Suydam stable equilibrium is defined by

$$\Sigma = \nabla p / \nabla p_s - 1 \tag{25}$$

with ∇p_s given by (15). The condition for non-oscillatory (i.e. stable) solutions is the Suydam condition $\Sigma_s \equiv \Sigma(r_s) < 0$.

For weak instability, i.e. Σ_s small and positive, the growth rates of the unstable modes can be obtained by equating the kinetic energy $\frac{1}{2} \int \rho\omega^2 \xi^2 \, r dr$ to the potential energy ΔW while retaining only the first term in g. To do this it is necessary to match the solution (24) on either side of $r = r_s$ as demonstrated by Pao [37]. An infinite set of eigenfunctions exists for each m and r_s, characterised by the radial node number n, and it was pointed out by Grad [35] that the growth rate γ decreases exponentially as n increases. This is well illustrated by Fig.6 of ref. [38]. Therefore in practice only the least localized mode n = 0 need be taken into account.

The growth rate of this mode is given by [35]

$$\gamma^2 \approx \frac{1}{\rho} \frac{2k^2}{K^2 r_s} \nabla p_s \, e^{-2\pi/\Sigma_s^{\frac{1}{2}}} \tag{26}$$

where the exponential factor expresses the radial width Δ of the eigenfunction [37]. Both γ and Δ are exponentially small as $\Sigma_s \to 0$. From the shape of the dashed curve shown in Fig.3 of ref. [39] it appears that γ should be very small for

$\Sigma_s < 1.4$, and this should also be true of the effective diffusion coefficient $\approx \gamma\Delta^2$. Another significant point brought out by the work of Goedbloed and Sakanaka (ref. [38] Fig.7) is that for fixed k/m, i.e. fixed r_s, the ideal MHD growth rate tends to an asymptotic limit as $m \to \infty$.

As Σ is increased well above zero the eigenfunctions become less and less localized and γ increases. Goedbloed [36] has generalized the Suydam criterion by including the linear and quadratic terms of g (second and third terms of (22)). The resulting eigenfunctions (equation (18) of ref. [36]) no longer depend only on the local value Σ_s and to estimate the growth rates it now becomes necessary to solve equation (18).

We have used the methods described in [17,18] to solve (18) numerically for a series of RFP equilibria. To investigate separately the effects from violating the Suydam criterion (16) we eliminate purely current-driven kink-modes by starting from the force-free Bessel function model; the field components (14) form a stable configuration for $\Theta < 1.587$ [22] and correspond to a $\beta_o = 0$ magnetic bottle. The bottle is pumped up with pressure by specifying $\Sigma = \Sigma(r)$ and solving equation (25) for p. Pressure equilibrium (1) is established by the method described in [20]. A specific choice of $\Sigma(r)$ involving $\Sigma > 0$ in the centre of the configuration represents the overheating effect mentioned earlier. We have used

$$\Sigma(r) = -\sigma_1 + \sigma_2 \, e^{-(r-r_1)^2/r_2^2} \quad , \tag{27}$$

and varied σ_1, σ_2 and r_1, r_2.

The results from several calculations made with the two different computer codes [17 and 18 resp.] are summarized in Figs.5 - 7. Fig.5 shows the increase in localization for m = 1 Suydam modes as the radial node number n increases, while Fig.6 depicts a similar but less drastic increase in localization with increasing m for n = 0 modes. Both sets of curves relate to the same equilibrium and the same value of r_s; the eigenfunctions of Figs.5 and 6 are similar to those shown in ref. [38] which were obtained for a $\Sigma(r)$

profile quite different from (27). In Fig.7 we show the calculated growth rates $\gamma(m = 1, k, n = 0)$ against the value Σ_s at the singular surface r_s for three different equilibria with $\Sigma(r)$ given by (27). For each equilibrium $\Sigma_s \to 0$ will result in the variation of ω with Σ_s as given by (26). When Σ_s is increased the growth rates now depend on the functional form of $\Sigma(r)$ rather than on Σ_s. For devices like ZETA and RFX the modes $n = 0$, $m = 1 - 5$ have growth times τ decreasing from 100 μsec down to 1 μsec as the maximum value of $\Sigma(r)$ increases from 1 to 10. The half-width Δ of the $n = 0$, $m = 1 - 5$ eigenfunctions (Fig.6) will typically be of the order 1 - 10% of a.

For a toroidal device such as ZETA or RFX, the allowable modes must satisfy the periodicity condition

$$k = \frac{\ell}{R_o} \quad , \ \ell = \pm 1, \pm 2, \ldots . \tag{28}$$

where R_o is the major radius. Every rational surface $r < a$ can become a singular surface r_s (equation (23)) by a suitable choice of m and k. However, of all possible values of m and k satisfying (23) and (28) only a finite number can in practice lead to instability, because non-ideal effects such as finite ion Larmor radius ρ_i and viscosity will stabilize short wavelength modes [39]. In Fig.8 we have indicated the distribution of the singular surfaces for modes $m = 1 - 5$ for a Bessel-function model with $\Theta = 1.5$ and an aspect ratio $R_o/a = 3$. There is a fairly close distribution near the centre although magic number effects cannot be excluded for the low-m modes. Beyond some point $r = a_1$ the modes of given m whose distribution becomes increasingly dense as $r \to a_R$ should be stabilized by the high shear.

The stabilizing effect of finite ion Larmor radius depends dynamically on Σ and on the ion pressure gradient and may be estimated from the work of Stringer (ref. [39] Fig.2). The critical m-value is likely in practice to be quite high, so justifying the assumption of a large number of competing localized modes with small radial separation from one another.

5. TURBULENT TRANSPORT IN THE CENTRAL CORE

Overheating of the central region of the RFP can occur during the current sustainment phase and a Suydam-unstable ($\Sigma > 0$) core of some radius a_1 is likely to develop. When a Suydam mode grows the field structure undergoes the Lagrangian transformation

$$\underline{r} \rightarrow \underline{r}^* = \underline{r} + \underline{\xi} \quad . \tag{29}$$

At some point during the growth the Jacobian $\left(\frac{\partial \underline{r}^*}{\partial \underline{r}}\right)$ can become zero or unbounded so that the transformation (29) itself becomes singular. This will happen when the radial Jacobian

$$\frac{\partial r^*}{\partial r} = 1 + \frac{\partial \xi}{\partial r}$$

approaches zero corresponding to

$$\left| \frac{\partial \xi}{\partial r} \right| = 1 \tag{30}$$

(the absolute value being appropriate because of the helical variation of ξ). From the study of Suydam unstable modes in the previous section we see that (30) will occur in the neighbourhood of the singular surface r_s when the maximum displacement $\xi(r_s)$ has grown to the order of its width Δ. If the initial amplitude $\xi(t = 0)$ is assumed to be of the order of the ion Larmor radius then the situation (30) will be reached after 1 - 4 growth times for devices like ZETA and RFX as $\xi(r_s) = \Delta$ varies from 1% to 10% of the radius a.

The topological changes that we expect to take place in the structure of the magnetic surfaces are indicated qualitatively in Fig.9. No change occurs until condition (30) is reached at some radius $r \approx r_s$, when there is a rearrangement in the neighbourhood of the singular surface. It will be seen from Fig.6 that both ξ and $|\partial\xi/\partial r|$ remain quite small outside this region, so that the surfaces should be only weakly distorted and their topology should remain invariant.

Modes whose m-number is sufficiently low to be unaffected by finite Larmor radius all have comparable growth rates, while $|\partial(\log \xi)/\partial r|$ increases with m, so that the change in topology should occur first for some radially-localized mode m > 1 which will not lead to a rearrangement of the entire inner region as apparently occurs during mini-disruptions in Tokamaks [5,6,7] and stellarators [8] where organized periodic relaxation oscillations are observed. Destruction of the local topology should rapidly flatten the pressure and temperature gradients in the neighbourhood of r_s, so raising $\Sigma(r)$ in the regions on either side and triggering off Suydam instabilities on adjacent magnetic surfaces by a sudden increase in their growth rate. This picture agrees qualitatively with a remark by Kadomtsev [14] who pointed out that pinches should exhibit a turbulent rather than an organized behaviour.

It is important for the conclusions of this paper that the instabilities occurring in Zone I should not give rise to turbulent MHD diffusion in Zone II (Fig.2). That is, the turbulence should not diffuse outwards. The argument is clearly valid for a single mode or for a linear combination of modes, since the radial derivatives of the eigenfunctions $\underline{\xi}_{mk}$ have too low an amplitude to affect the topology of the magnetic surfaces in Zone II and should simply lead to a random motion like the random oscillations of an elastic solid. However we cannot yet exclude the possibility that turbulent MHD energy generated in Zone I might undergo non-linear coupling into stable Alfvén waves whose singular surfaces are located in Zone II, and these could damage the topology.

Another unresolved question is whether there is any tendency for the magnetic surfaces in Zone I to "heal" themselves automatically once the pressure distribution has been flattened, or whether the magnetic field remains permanently ergodic as in the "tangled discharge model" of Rusbridge [40,41] when part of the excess pressure might be continually removed by longitudinal electron thermal conduction. We shall however assume here that healing does take place.

The usual γ/k^2 estimate for the instability diffusion coefficient, i.e.

$$D_I \simeq \gamma \Delta^2 \tag{31}$$

is difficult to apply since D_I is exponentially small near $\Sigma = 0$ from equation (26). A marginal stability argument [30] is also not straightforward in our case since it seems likely that once the magnetic surfaces have been locally destroyed, which will occur for some finite value $\Sigma > 0$, rapid flattening of the local pressure and temperature profiles will take place so that $\Sigma \to -1$ (25). We envisage that this hysteresis effect will lead to an irregular sequence of local explosive instabilities or "micro-disruptions", with the marginal stability criterion $\Sigma(r) = 0$ applying only as an approximate time average.

The expression (31) may be compared with the classical [42] cross-field diffusion coefficient D_o and the poloidal Bohm diffusion coefficient D_θ. For typical values $B_\theta = 0.25$ T, $\beta_o = 0.25$, $\log \Lambda = 10$ we have (T_* in eV)

$$D_o = \frac{\beta}{4\mu_o} \eta_\perp^o = 50\ T_*^{-3/2}\ m^2 s^{-1} \tag{32}$$

$$D_\theta = \frac{1}{16} \frac{kT}{eB_\theta} = 0.25\ T_*\ m^2 s^{-1} \quad . \tag{33}$$

Evidently $D_I << D_o$ as $\Sigma \to 0$, but for the faster-growing Suydam modes, say

$$\gamma \sim 10^4 - 10^5\ s^{-1} \quad , \quad \Delta \sim 0.01 - 0.05\ m$$

we find that D_I lies in the range $1 - 250\ m^2 s^{-1}$. This is to be compared with $D_o = 5.10^{-2} - 6.10^{-3}\ m^2 s^{-1}$ and $D_\theta = 25 - 100\ m^2 s^{-1}$ in the temperature range $T_e = 100 - 400$ eV.

To simulate the turbulent diffusion numerically it is convenient to choose a simple analytic form for the coefficients in (6) - (8):

$$D_T = \begin{cases} C_T \dfrac{\Sigma}{1+\Sigma} D_\theta & (\Sigma > 0, \text{ unstable}) \\ 0 & (\Sigma < 0, \text{ stable}) \end{cases} \tag{34}$$

where C_T is an adjustable constant. This switches on the diffusion like a

thermostat whenever $\Sigma > 0$, but the switch-on process is smoothed out to some extent both for reasons of numerical stability and also in partial accordance with (26). The scaling of D_T serves as a convenient reference point since both D_I and D_θ are of the same order; in fact using the Bennett pinch relation $NT \propto \beta_\theta I_z^2$ we see that

$$D_I \propto a^2(B/\sqrt{N}) \quad , \quad D_\theta \propto D_I(\beta_\theta/\sqrt{N})$$

so that for pinch devices with similar magnetic field B, line density N and β_θ the main dependence is on a^2. However we emphasize that the specific choice (34) has little influence on the results obtained so long D_T is large since Σ simply adjusts itself to the level needed to carry away the excess pressure.

Turbulent diffusion of the plasma relative to the magnetic field is represented in the ATHENE 1 code by the coefficient D_T' in equation (6), which also leads to turbulent heating that can be divided in arbitrary proportion between the ions and electrons and conserves the total energy [19]. The coefficients D_T'', D_T''' represent turbulent thermal conduction. Calculations have been carried out [43,44] in which the corresponding constants C_T', C_T'', C_T''' were varied over a wide range, the allocation of heat between ions and electrons altered, and the functional form (34) changed, Provided $D_T >> D_o$ the results are not seriously influenced by these parameters and for the calculations reported in this paper the choice made was $C_T' = C_T'' = C_T''' = 1$, with the turbulent heat production divided equally between electrons and ions.

6. ELECTRON THERMAL TRANSPORT IN ZONE II

The enhanced transport of plasma and energy across the magnetic field will establish flat density and temperature profiles in Zone I, the Suydam unstable core of the RFP. The calculations referred to at the end of the last section have demonstrated, not unexpectedly, that the details of the turbulent transport do not greatly influence the performance of the RFP, i.e.

the stable configuration time τ_c and the predicted temperatures. These mainly depend on the confinement Zone II.

The effect of turbulence in Zone I is to steepen the gradients in Zone II, but provided that the MHD turbulence does not spread outwards the most this should do is roughly to double the particle and energy loss rates. It is also worth remarking that the level of turbulence in Zone I is controlled by the joule heating rate and by the rate at which heat can be transported across Zone II, and should fall as the temperature rises. This is in accordance with results on ZETA reported by Butt and Newton [45], who found that during the quiescent period the fluctuation level $\Delta B_\theta/B_\theta$ scaled as I_z^{-3}.

As mentioned in the Introduction the configuration time τ_c is determined by the decay of B_z flux, either the negative flux ψ_- as in ZETA, or the positive flux ψ_+ as in RFX. Now the major part of the B_z energy loss takes place in Zone II, so that since $\eta_{\parallel} \sim T^{-3/2}$ the value of τ_c will depend strongly on the T_e profile of this zone and therefore on the electron thermal conductivity together with any other heat loss processes that may be important. To emphasize this point, we have plotted in Fig.10 the rate $rE_\theta J_\theta$ at which the B_z energy of a cylindrical shell of radius r is transferred to the plasma. The full curve shows the initial transfer rate $r\eta_{\parallel} J_\theta^2$ for the Bessel function model ($\eta_{\parallel}$ = constant), while the dashed curve shows the rate computed during a run which has a hot core and a cooler region outside.

Unfortunately there is little experimental evidence as yet concerning the scaling of electron thermal conductivity with T, B, n and radius a in RFP geometry. Experiments on Tokamaks [5,6,7,9] indicate that the ion thermal losses are neo-classical while the electron thermal losses are anomalous. Several authors [9,10] have derived empirical scaling laws for the energy containment time τ_E from the available Tokamak measurements and we have used the results of ref. [10] in order to bracket the predicted performance of the RFP.

The most convenient theoretical definition of the energy containment time in our calculations is

$$\tau_E = \frac{W}{L} \tag{35}$$

with

$$W = \int_0^a nk(T_e + T_i/Z_{eff})rdr$$

and L the total loss rate, which in the present calculations is approximately

$$L = a(F_e + F_i)_{r=a} \tag{36}$$

where $F_{e,i}$ are the thermal fluxes to the wall, since Bremsstrahlung is small and impurity losses are not yet included in the code. In experimental work it is difficult to measure L, and since Tokamaks reach an approximately steady state in which loss rate L balances the ohmic heating rate Ω and the configuration time $\tau_c \approx 10\ \tau_E$ [46], the alternative definition

$$\tau_E = \frac{W}{\Omega} \tag{37}$$

is adopted in practice where

$$\Omega = I_\phi V$$

and V is the loop voltage. It would not however be practical to use definition (37) for the RFP calculations since a steady state is not reached.

The Tokamak scaling laws [9,10,46] may be expressed in various ways. They do not directly relate to the RFP which has a lower toroidal field B_z but a stronger shear. The most plausible comparison seems to be between a Tokamak and a RFP with the same temperature, poloidal field and minor radius, other parameters being disregarded, although it is not known which of the two geometries this comparison would favour. Since the Tokamak scaling laws provide an overall energy containment time τ_E rather than a detailed functional form for the electron thermal conductivity, the approach that we have adopted is to choose two alternative analytic expressions for

the anomalous electron thermal conductivity in equation (7), each with an arbitrary multiplying constant, and to carry out a series of calculations in which τ_E is determined from equation (35). The multiplying constants are then chosen to bracket the Tokamak data. This procedure should be valid even if part of the energy loss is due to processes other than thermal conductivity, for example to impurity radiation.

The alternative forms chosen were

$$\underline{\text{Pseudoclassical}} \qquad D_a = C_e D_e^o \tag{38}$$

$$\underline{\text{Poloidal Bohm}} \qquad D_a = C_\theta D_\theta \tag{39}$$

where $D_e^o = \kappa_{\perp e}^o / nk$ is the diffusion coefficient corresponding to classical transverse thermal conductivity, (classical and neoclassical are essentially the same in the RFP), while D_θ is given by (33). The coefficients used in the calculations reported in Sections 6 and 7 covered the ranges $C_e = 0 - 100$, $C_\theta = 0 - 0.15$.

7. ZETA CALCULATIONS

The main parameters of the ZETA apparatus are given in Table I. The time variation of the toroidal current is shown in Fig.1 of ref. [12] and indicates a quiescent phase lasting 1.5 msec. The initial field profiles used in our calculations were constructed from experimental data given in Fig.4 of ref. [11] and Fig.11 of ref. [12]. We have normalized the B_z values measured at $R = R_o + a$ to the vertical plane $R = R_o$ (where R is distance from the toroidal axis so that $B_z \sim 1/R$). The measured density and temperature profiles were flat near the centre [27], with $T_e = 100$ eV on axis; little is known about T_i so we assume that initially $T_i = T_e$ [12,27]. The plasma was surrounded by a stainless steel bellows liner [27] with poloidal copper rings. The toroidal liner resistance $R_z = 2.5 \times 10^{-2}$ Ω and poloidal resistance $R_\theta = 3.9 \times 10^{-4}$ Ω are included in the calculations and have the effect of shunting the plasma currents

at the liner radius so affecting the decay of the ψ_- flux. This requires a modification to the components η_{zz}, $\eta_{\theta\theta}$ and $\eta_{z\theta}$ of the resistivity tensor at the boundary point.

Results from the ZETA calculations are summarized in Figs.11,12 and Table II. Although the anomalous electron thermal conductivity was varied over a wide range using both expressions (38) and (39), we see that there is only a rather small change in the predicted energy containment time τ_E and the configuration time τ_c, defined here to be the time at which B_z at r = a goes through zero so that the discharge is expected to be unstable due to a pitch minimum at the wall. Thus ZETA appears to provide very little information about the anomalous electron thermal conductivity in Zone II. On the other hand the calculated change in the reversed B_z profile shown in Fig.11 agrees quite well with the measured results, and the calculated time variation of the electron temperature on axis is within the experimental error bars, so giving a reasonable degree of confidence in the theoretical model. A value $Z_{eff} = 2.5$ gives better agreement with Fig.5 of ref. [12] than $Z_{eff} = 1$.

As the reversed field gradually disappears (Fig.11) the shear is lowered and Fig.13 shows how this leads to a marked increase of the Suydam parameter Σ in the outside region. We have performed stability calculations with the codes [17,18] on the ZETA configurations at t = 0.5, 1.0 and 1.5 msec, although these calculations are not conclusive for modes whose singular surfaces lie in the outside region, since the stability of such modes is strongly influenced by the exact distance d between the liner at r = a and the conducting shell at r = a + d. The boundary condition $\xi(a) = 0$ ought therefore to be replaced by $b_r(a + d) = 0$, where b_r is the perturbed radial field, so that the vacuum region $a < r < a + d$ contributes to ΔW (equation 19).

Fig.14 shows the eigenfunctions of three typical m = 1 Suydam unstable modes both being of the type shown in Fig.6. Fig.14 also shows the development of a mode whose singular surface lies in a nearly Suydam stable zone. This

mode, m = 1 and ℓ = - 5, stable at t = 0.5 msec, becomes progressively unstable; at t = 1.5 msec the mode is not localized at all and it might cause a kink-like loss of plasma. Such a result can be derived from the interpretation of new results from ZETA by Butt and Newton [47] who suggest that the end of the quiescent period occurs when the pressure limit β_s shown in Fig.3(b) is exceeded because of the decay of Θ.

8. PREDICTIONS FOR RFX

Table I also shows the parameters for a proposed new apparatus RFX which is intended to have a larger minor radius a, programmable wall fields, and a larger toroidal current for stable operation than ZETA. Since the line density N appears from experiments to be a critical parameter for pinch operation, we have for the purpose of comparison assumed the same value 2.10^{19} m^{-3} as in ZETA so that the central density is lower in the ratio a^{-2}. The calculations start off from the magnetic field configuration (14) with parabolic density and temperature profiles; initially a very low temperature $T_e = T_i$ = 10 eV is assumed on axis in order not to disturb the initial Bessel-function configuration appreciably, but the temperature quickly rises in the first few timesteps.

The reversed flux ψ_- can be supported by programming E_θ in various ways; a simple choice is to maintain the ratio

$$\frac{B_z(a,t)}{B_z(o,t)} = \frac{B_z(a,o)}{B_z(o,o)} = J_o(2\Theta) \qquad (40)$$

of the wall field to the field on axis, where J_o is the Bessel function. The toroidal current I_z can either be kept constant or allowed to decrease in a controlled fashion in order to prolong the stable period.

Table II shows the predicted axial temperatures for various choices of the transport coefficients. To emphasize the difference between classical

and strongly anomalous thermal transport we indicate in Figs.15 and 16 the profiles of T_i and B_z for Cases 1 and 12. The dashed curves (classical case 1) show that little B_z energy has been consumed by the plasma in Zone II which is relatively hot. Strong anomalous thermal losses cool down Zone II, causing ψ_+ to decay so that the configuration pinches. For RFX the configuration time $t = \tau_c$ is defined to be the time at which the pinch parameter Θ exceeds Θ_I, so leading to an m = 1 gross kink instability [26] (see Figure 3(b)).

Empirical Tokamak scaling laws [10,46] predict an RFX energy containment time $\tau_E \approx 26$ ms corresponding to $C_\theta \approx 0.05$ or $C_e \approx 50$. Since there is considerable variation between different Tokamak discharges, as well as uncertainty in the comparison between RFP and Tokamak and in the extrapolation of the present experimental results to radii as large as a = 0.6 m, we have extended the calculations to $C_\theta = 0.15$ and $C_e = 100$.

The variation in predicted performance is greatest for the configuration time τ_c, whereas for given Z_{eff} the predicted axial temperature variation is only of order 10%. To increase τ_c the rate at which the discharge pinches can be reduced by letting the current I_z decay. Several calculations have been performed in which $\dot{I}_z/I_z$ is either kept constant or proportional to $\dot{\psi}_+/\psi_+$. The resulting rate of pinching is illustrated in Fig.17, which plots the field reversal ratio F of equation (12) against the pinch parameter Θ of equation (11). The solid line to the left represents the $\beta = 0$ Bessel function model for which

$$F = \frac{J_o(2\,\Theta)}{J_1(2\,\Theta)}\,\Theta \quad . \tag{41}$$

By adding pressure to this model, but keeping $\Sigma < 0$, one can obtain [47] a kink-stable high-β configuration which is indicated by the solid line to the right. The route taken by ZETA (case 12) is compared with three RFX discharges, the first two (with constant I_z) being cases 1 and 12 of Figs.15 and 16, while in the third discharge (case 12a) $\dot{I}_z/I_z = 0.6\ \dot{\psi}_+/\psi_+$ with the parameters otherwise the same as in case 12. The configuration time is prolonged to $\tau_c = 22$ ms.

in case 12a compared to 10 ms in case 12, but at the expense of a somewhat lower axial temperature T_e = 501 eV at 20 ms compared to 702 eV.

Trying various forms of field programming we have found that Θ can remain below Θ_I for as long as 30 - 40 msec. Whether a discharge could remain kink-stable throughout this period would have to be studied in detail. The criterion $\Theta < \Theta_I(\beta_o)$ [26] can only serve as a guide. Sakanaka and Goedbloed [31] have made an interesting comparison betwen an unstable and a stable equilibrium whose profiles [Fig.18 in ref. 31] hardly differ. They conclude categorically that "answers about which configurations are bad and which are good with respect to stability cannot be given".

The main conclusion from these calculations is that, on the basis of a wide range of reasonable predictions for the electron thermal conductivity in Zone II, the RFX apparatus should be able to attain central temperatures of order 500 - 600 eV, $\beta_\theta \approx 13\%$, with a stable lifetime $\tau_c \approx 15 - 25$ ms.

9. CONCLUDING REMARKS

We have studied the current sustainment phase of a slow reversed field pinch on the basis of theory, numerical calculations and available experimental data. This has led to an RFP model qualitatively sketched in Fig.2. The turbulent behaviour that is expected to arise from instabilities localized in the central zone I is found not to degrade the performance of the RFP unduly, and although the details of this MHD turbulence remain unknown their precise form is not expected to be important. The model emphasizes that, in general, the predicted performance is likely to depend on the electron thermal conductivity in the confining layer II. At present there is little experimental evidence on anomalous transport coefficients in RFP geometry. We have therefore used alternative analytic expressions with adjustable coefficients to narrow the uncertainty concerning the behaviour of the plasma in this zone. For calculations on ZETA this has led to an acceptable agreement with

the experimental results, largely because temperature in ZETA was sufficiently low not to be greatly affected by electron thermal conduction.

The calculations on RFX demonstrate a substantial improvement in performance over that of ZETA. Programming of the wall fields ensures that the configuration time is determined by the decay of positive flux ψ_+ rather than the decay of negative flux ψ_- as in ZETA. Our calculations indicate that RFX discharges with a stable lifetime of 15 - 25 ms should reach 500 - 600 eV with a $\beta_\theta \sim 13\%$.

Compared to the 1DMHD diffusion codes that are now used for studying Tokamaks the physics model employed in this paper is still in a relatively embryonic state and additional effects will be included in due course. The main uncertainty in our predictions is probably the implicit assumption of a good set of nested magnetic surfaces, concentric with the wall, in the outer region of the pinch. The configuration time τ_c is sensitive to the electron temperature in this outer region, and a lack of concentricity causing magnetic field lines to cut the wall could lower T_e by longitudinal thermal conduction and so reduce τ_c. Adjustment of the axis of the current channel by means of a programmable vertical field may therefore be needed if the performance is to reach the theoretical predictions.

REFERENCES

[1] Bodin, H.A.B., Pulsed High Beta Plasmas, Pergamon Press (1976) 39.
Bodin, H.A.B. et al., in Plasma Physics and Controlled Nuclear Fusion Research (Proc.5th Int.Conf.Tokyo,1974) 3, 631.

[2] Rosenbluth, M.N., 2nd Int.Conf.On the Peaceful Uses of Atomic Energy (Proc.Conf.Geneva,1958) 31, UN, 85.

[3] Suydam, B.R., 2nd Int.Conf.On The Peaceful Uses of Atomic Energy (Proc.Conf.Geneva,1958) 31, UN, 157.

[4] Watkins, M.L., Hughes, M.H., Roberts, K.V., Keeping, P.M., Killeen, J., ICARUS, A One-Dimensional Plasma Diffusion Code, Vol.16 of Methods in Computational Physics, Academic Press (1976).

[5] Karger, F. et al., in Plasma Physics and Controlled Nuclear Fusion Research (Abstracts 6th Int.Conf.Berchtesgaden,1976) CN-35/A7.

[6] TFR Team, ibid, CN-35/A8.

[7] Mirnov, S.V., Semenov, I.B., ibid, CN-35/A9.

[8] Wendelstein VIIA Team, ibid, CN-35/D2.

[9] Daughney, C.C., Nucl.Fusion 15 (1975) 967.

[10] Hugill, J., Sheffield, J., Empirical Tokamak Scaling (1976), submitted to Nucl.Fusion.

[11] Robinson, D.C., Boland, B.C., King, R.E., Pease, R.S., in Plasma Physics and Controlled Nuclear Fusion Research (Stockholm, 1967).

[12] Robinson, D.C., King, R.E., in Plasma Physics and Controlled Nuclear Fusion Research (Proc.3rd Int.Conf.Novosibirsk,1968) I, 263.

[13] Taylor, J.B., Phys.Rev.Lett. 33 (1974) 1139.

[14] Kadomtsev, B.B., in Plasma Physics and Controlled Nuclear Fusion Research (Abstracts 6th Int.Conf.Berchtesgaden,1976) CN-35/B1.

[15] Robinson, D.C. et al., in Controlled Fusion and Plasma Physics (Proc.5th Europ.Conf.Grenoble,1972) II, 47-158.

[16] Robinson, D.C., Rusbridge, M.G., Plasma Physics 11 (1969) 73.

[17] Appert, K., Berger, D., Gruber, R., Roberts, K.V., Troyon, F., Comp.Phys.Comm. 10 (1975) 11.

[18] Crow, J., Robinson, D.C., 2nd Conf.on Pulsed High Beta Plasmas (Garching,1972) C1.

[19] Rusbridge, M.G., Plasma Physics 11 (1969) 35.

[20] Roberts, K.V., Christiansen, J.P., Long, J.W., Comp.Phys.Comm. 10 (1975) 264.

[21] Newcomb, W.A., Ann.Phys. 10 (1960) 232.

[22] Voslamber, D., Callebaut, D.K., Phys.Rev. 128, no.5 (1962) 2016.

[23] Furth, H.P., Killeen, J., Rosenbluth, M.N., Phys.Fluids 6 (1963) 459.

[24] Coppi, B., Greene, J.M., Johnson, J.L., Nucl.Fusion 6 (1966) 101.

[25] Gibson, R.D., Whiteman, K.J., Plasma Physics 10 (1968) 1101.

[26] Robinson, D.C., in Plasma Physics and Controlled Nuclear Fusion Research (Abstracts 6th Int.Conf.Berchtesgaden,1976) CN-35/E2.

[27] Robinson, D.C., Private Communication (1976).

[28] Dibiase, J.A., Ph.D.Thesis, Report UCRL-51591 (1974).

[29] Butt, E.P. et al., in Plasma Physics and Controlled Nuclear Fusion Research (Proc.5th Int.Conf.Tokyo,1974) 3, 417.

[30] Manheimer, W.M., Chu, K.R., Ott, E., Boris, J.P., Phys.Rev.Lett. 37 (1976) 286.

[31] Sakanaka, P.H., Goedbloed, J.P., Phys.Fluids 17 (1974) 919.

[32] Clayton, D.D., Principles of Stellar Evolution and Nucleosynthesis, McGraw-Hill (1968).

[33] Robinson, D.C., Plasma Physics 13 (1971) 439.

[34] Goedbloed, J.P., Hagebeuk, H.J.L., Phys.Fluids 15 (1972) 1090.

[35] Grad, H., Proc.Nat.Acad.Sci. 70 (1973) 3277.

[36] Goedbloed, J.P., Phys.Fluids 16 (1973) 1927.

[37] Pao, Y-P., Phys.Fluids 17 (1974) 600.

[38] Goedbloed, J.P., Sakanaka, P.H., Phys.Fluids 17 (1974) 908.

[39] Stringer, T.E., Nucl.Fusion 15 (1975) 125.

[40] Rusbridge, M.G., A model of field reversal in the diffuse pinch (1977), to appear in Plasma Physics.

[41] Rusbridge, M.G., Lees, D.J., Saunders, P.A.H., Nucl.Fusion Suppl.Pt.3 (1962) 895.

[42] Spitzer, L., Physics of Fully Ionized gases, Interscience Publishers, New York (1965).

[43] Christiansen, J.P., Roberts, K.V., Pulsed High Beta Plasmas, Pergamon Press (1976) 317.

[44] Christiansen, J.P., Roberts, K.V., 2nd Europ.Conf.on Computational Physics (Proc.Garching,1976) G3.

[45] Butt, E.P., Newton, A.A., Pulsed High Beta Plasmas, Pergamon Press (1976) 425.

[46] Hugill, J., Sheffield, J., Private Communication (1976).

[47] Newton, A.A., Li Yin-An, Long, J.W., Yeung, B.C., Pulsed High Beta Plasmas, Pergamon Press (1976) 323.

TABLE I

Main parameters for ZETA and RFX

	Symbol	ZETA	RFX
Radius of liner [m]	a	0.5	0.6
Radius of shell [m]	a+d	0.535	0.63
Major radius [m]	R_o	1.84	1.8
Current [MA]	I_z	0.42	0.7
Toroidal Flux [Vs]	ψ	0.088	0.183
Line density [m^{-1}]	N	2×10^{19}	2×10^{19}
B_z on axis [T]	B_o	0.33	0.55
n on axis [m^{-3}]	n_o	5×10^{19}	3.2×10^{19}
n at liner [m^{-3}]	n_a	10^{19}	1.2×10^{19}
$T_{e,i}$ at liner [eV]	$T_{e,i}(a)$	20	8
Pinch parameter at t=0	Θ	1.36	1.44
Field reversal ratio at t=0	F	- 0.145	- 0.53

TABLE II

Calculations on ZETA and RFX

CASE	$(Z,A)_{eff}$	Electron thermal Transport	ZETA					RFX				
			τ_E	τ_c	T_e	T_i	β_θ	τ_E	τ_c	T_e	T_i	β_θ
1	(1,1)	Classical	1.93	1.60	146	126	12.7	85	100	598	518	16.4
2		$C_\theta = 0.05$	1.62	1.68	145	125	13.1	27	40	513	474	13.5
3		$C_\theta = 0.1$	1.53	1.68	144	125	12.8	21	40	472	447	12.6
4		$C_\theta = 0.15$	1.47	1.6	144	125	12.5	17	32	443	426	12.0
5		$C_E = 50$	1.36	1.50	144	125	11.8	24	35	543	489	13.0
6		$C_E = 100$	1.16	1.39	140	123	11.3	19	22	520	476	12.2
7	(2.5,4)	Classical	1.80	1.16	198	112	12.1	81	60	896	645	16.9
8		$C_\theta = 0.05$	1.68	1.16	196	113	11.9	19	25	720	609	13.5
9		$C_\theta = 0.1$	1.56	1.15	195	113	11.8	14	20	651	585	12.5
10		$C_\theta = 0.15$	1.49	1.2	193	113	11.6	11.5	15	608	565	11.9
11		$C_E = 50$	1.01	1.07	187	113	10.6	15	12	754	617	12.5
12		$C_E = 100$	0.82	1.02	174	113	9.6	12	10	702	603	11.8

Data from 12 calculations on ZETA and RFX using various values of the scaling factors C_θ and C_E in the electron thermal conductivity coefficient (equations 38 and 39). The energy containment time τ_E in ms, β_θ in % and the axial temperatures in eV are given at t = 1.5 ms for ZETA and at t = 20 ms for RFX. The configuration time τ_c for ZETA is defined to be the time when B_z at the liner goes through zero, while for RFX is is the time at which Θ exceeds Θ_I (see Figure 3(b)).

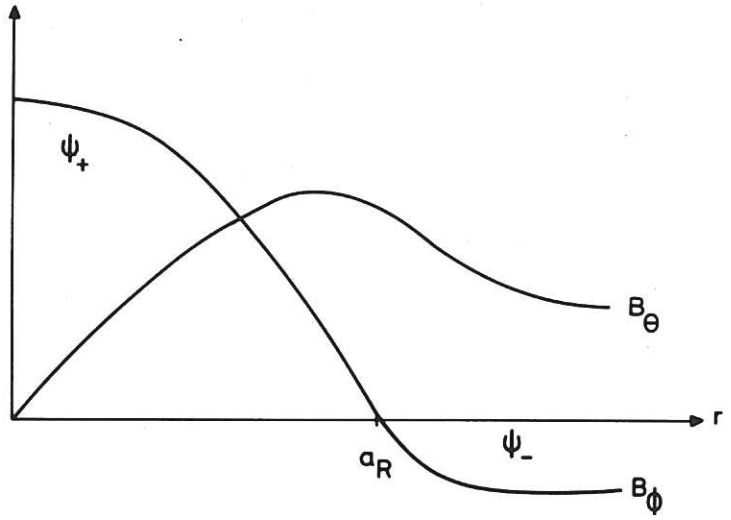

Figure 1 Radial profiles of the toroidal (B_ϕ) and the poloidal (B_θ) field components of a reversed field pinch (RFP). ψ_+ is the positive flux trapped inside the field reversal point a_R and ψ_- is the negative flux at the outside.

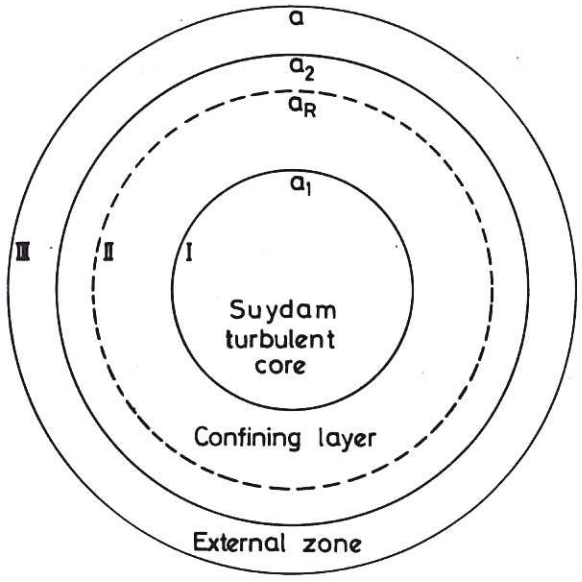

Figure 2 Qualitative diagram of an RFP model divided into regions I,II,III of radii a_1,a_2,a respectively. The field reversal point a_R may extend into the exterior zone.

CLM-P484

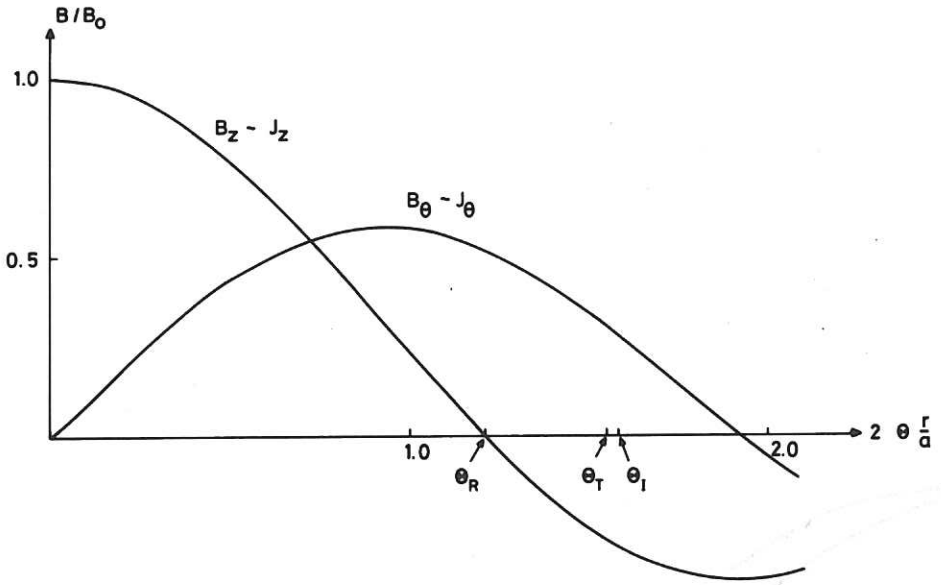

Figure 3(a) Radial profiles of magnetic field and current density components for the Bessel-function model. A given value of Θ (equation 11) corresponds to a fixed wall radius r = a. The configuration is MHD unstable for $\Theta > \Theta_I = 1.587$ and tearing mode unstable for $\Theta > \Theta_T = 1.552$. The reversal point is $\Theta_R = 1.202$.

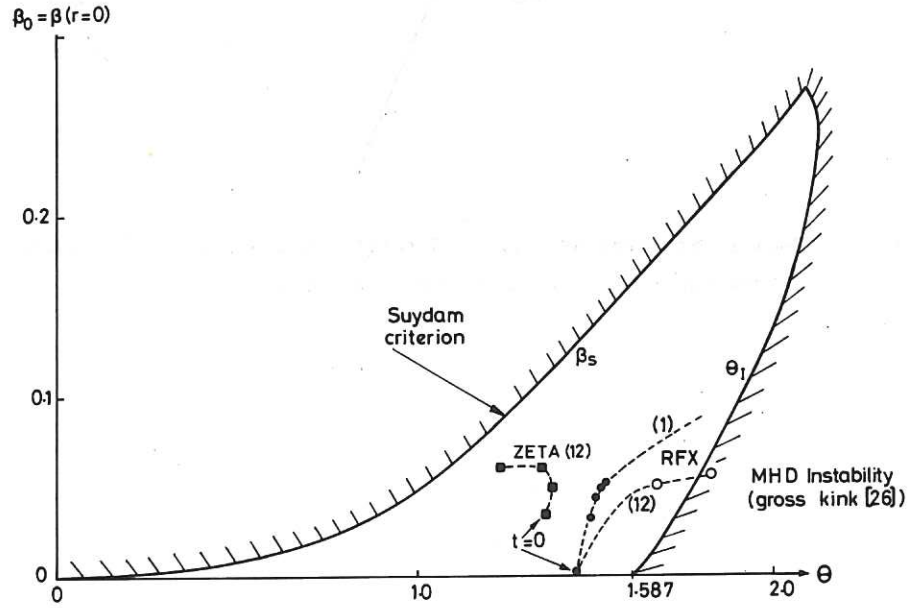

Figure 3(b) The curve labelled β_S indicates the maximum Suydam-stable central value β_o obtained by integration of equation (15) and allowing for pressure equilibrium. The curve labelled Θ_I calculated by Robinson [26] shows the maximum value of Θ at which the pressure inflated Bessel-function configuration is marginally stable against ideal MHD gross kink modes. The dashed curves show the calculated routes taken by ZETA and RFX for cases (1) and (12) (see Table II and Figure 17). The time spacing between the points is the same as in Fig.17.

CLM-P484

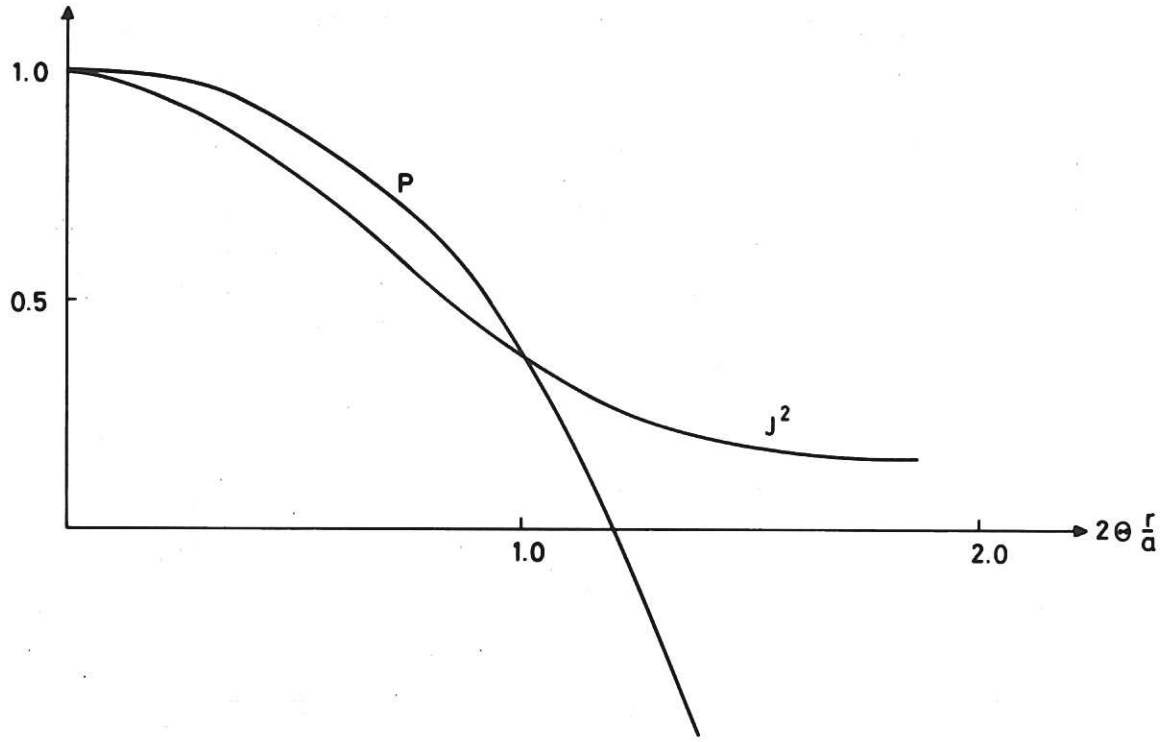

Figure 4 Radial variation of pitch and total heating rate $\sim J^2$ for the Bessel function model in normalized units.

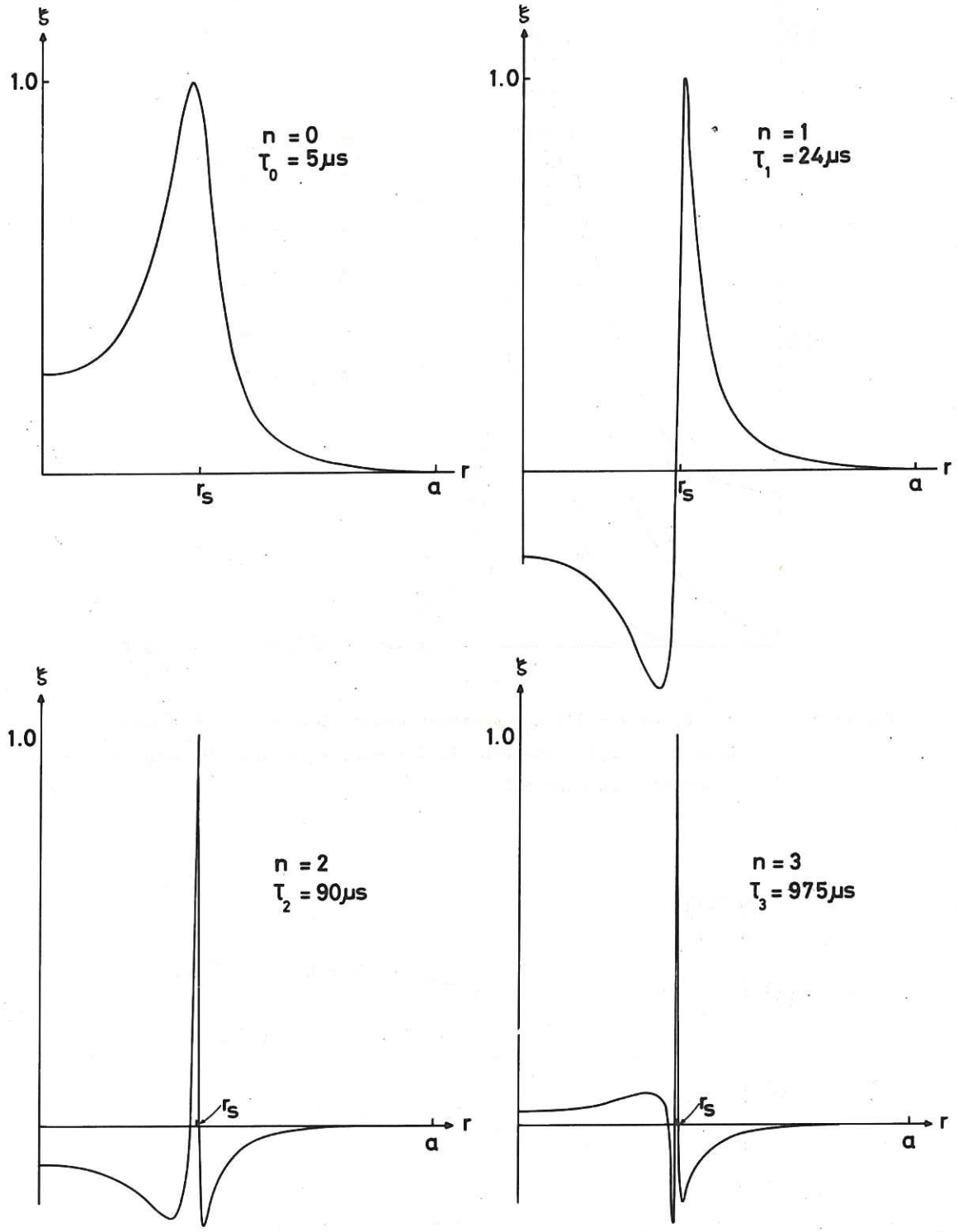

Figure 5 m = 1, ka = - 5/3 eigenfunctions of Suydam unstable modes. n denotes radial node number. The position of the singular surface r_s is shown. $\Sigma(r)$ is given by (27) with $\sigma_1 = -0.9$, $\sigma_2 = 10$, $r_1 = 0.3a$, $r_2 = 0.3a$.

CLM-P484

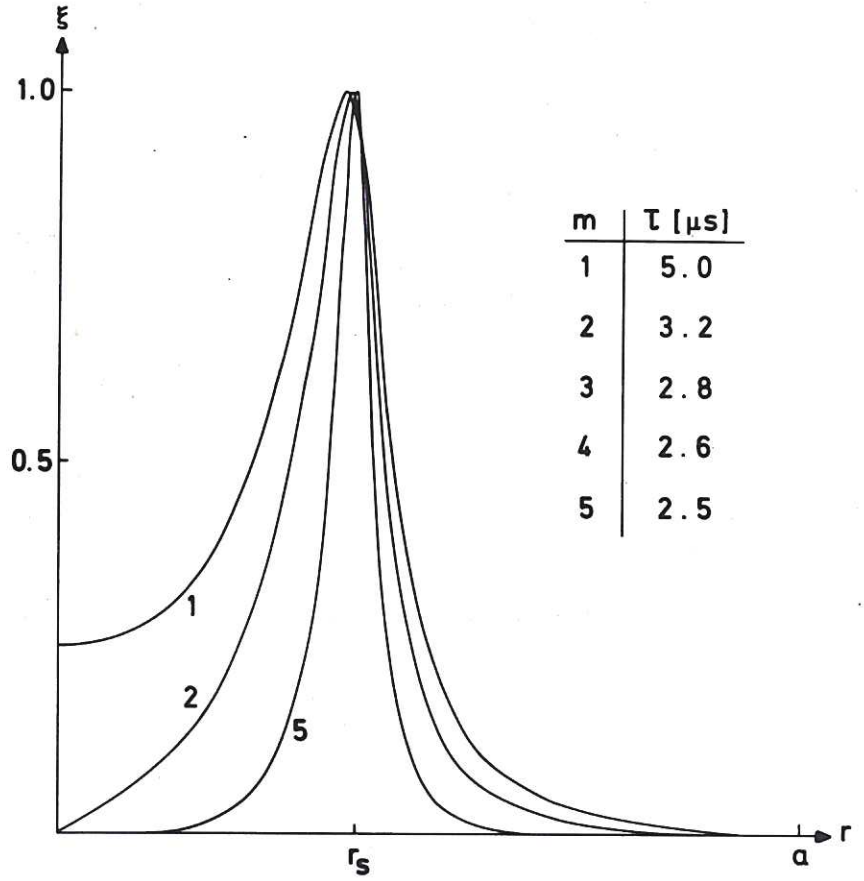

Figure 6 n = 0, ka = - 5/3 m eigenfunctions of Suydam unstable modes with m = 1,2,5. The equilibrium parameters are the same as those used in Figure 5.

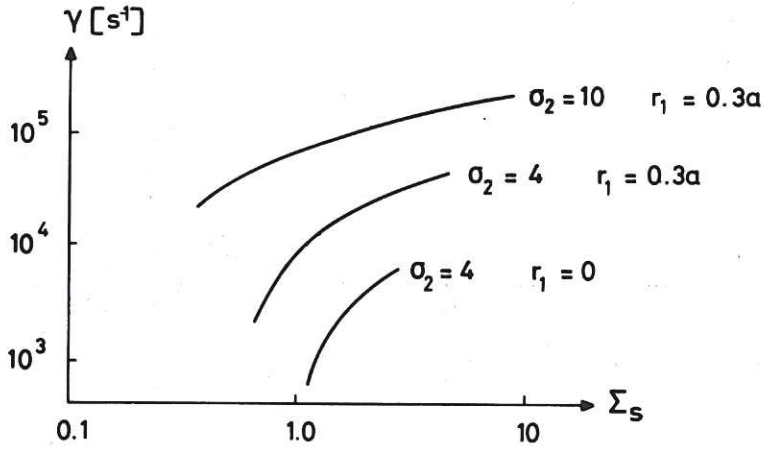

Figure 7 Growth rates γ for three equilibria where Σ(r) is given by (27). $\sigma_1 = -0.9$, $r_2 = 0.3a$. The growth rates correspond to RFX with $B_o = 0.55$ Tesla and $n_o = 3.2 \times 10^{19}$ m^{-3}. Σ_s is the value of $\Sigma(r_s)$.

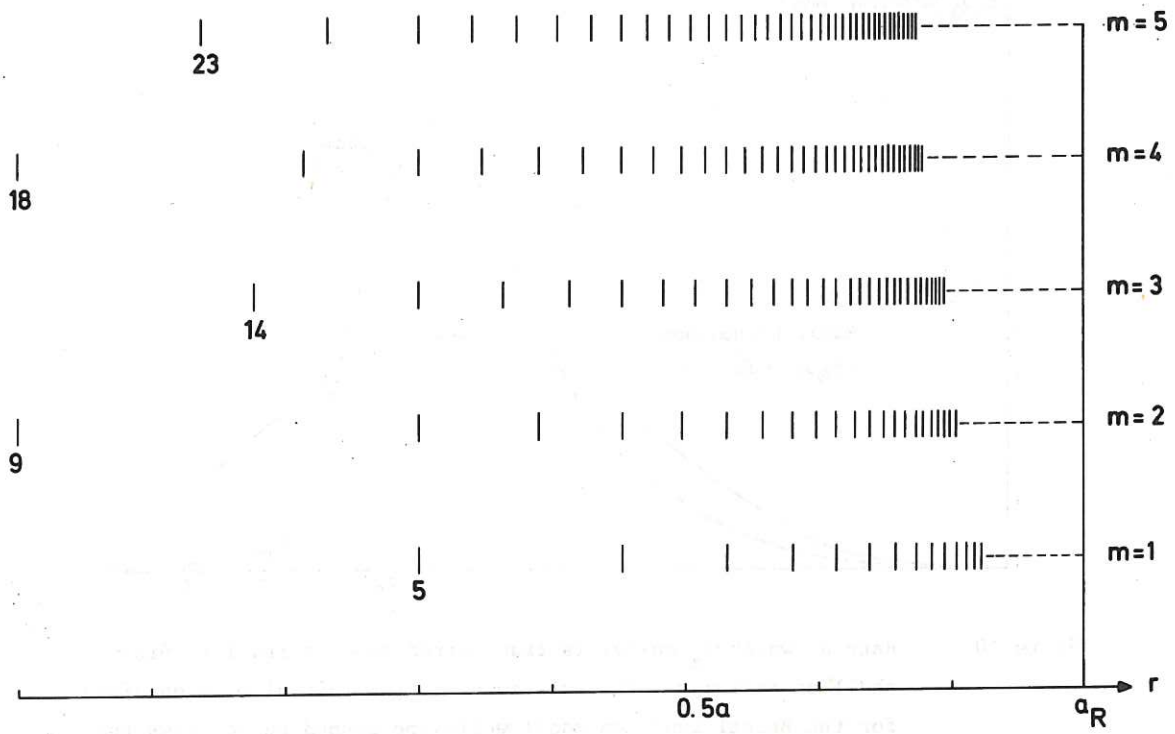

Figure 8 Positions of singular surfaces r_s for the Bessel function model (Fig.3(a)) with $\Theta = 1.5$ shown for modes with $1 \leq m \leq 5$; k satisfies (23) and (28) with an aspect ratio $R_o/a = 3$. The lowest value of $-\ell$ is indicated to the left for each value of m. The distribution of singular surfaces becomes increasingly more dense as $r \to a_R$; it is indicated by a dashed line. Singular surfaces $r_s > a_R$ are not shown.

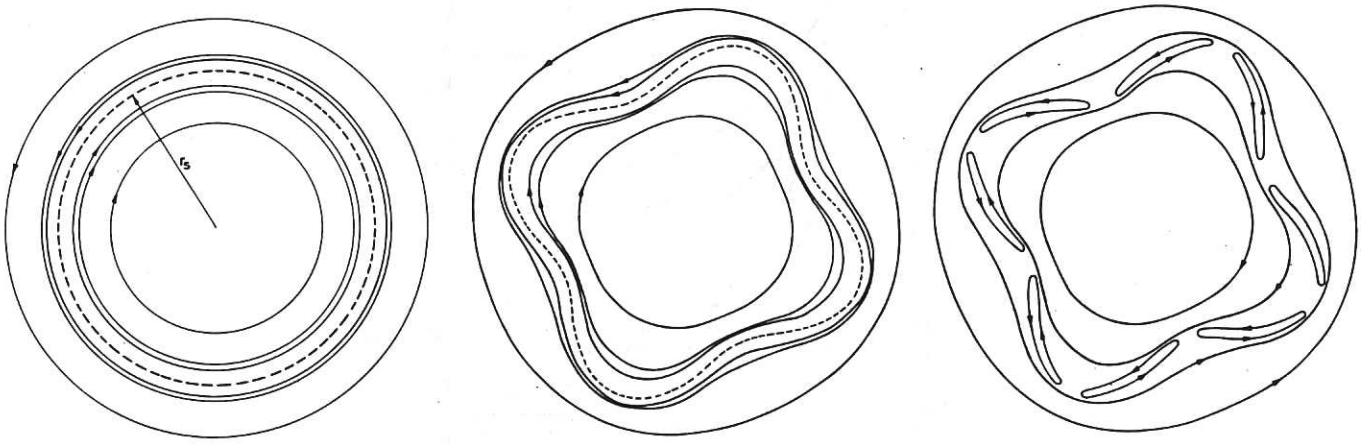

Figure 9 Qualitative interpretation of the transformation (29) corresponding to $\left|\frac{\partial \xi}{\partial r}\right| \to 1$ (Figures 9(a) and 9(b)) as a result of an unstable localized m = 4, n = 0 mode. After cutting and rejoining the field lines the field structure in Figure 9(c) is established. The arrows show the directions of the field component transverse to the field direction at r_s (dashed curves).

CLM-P484

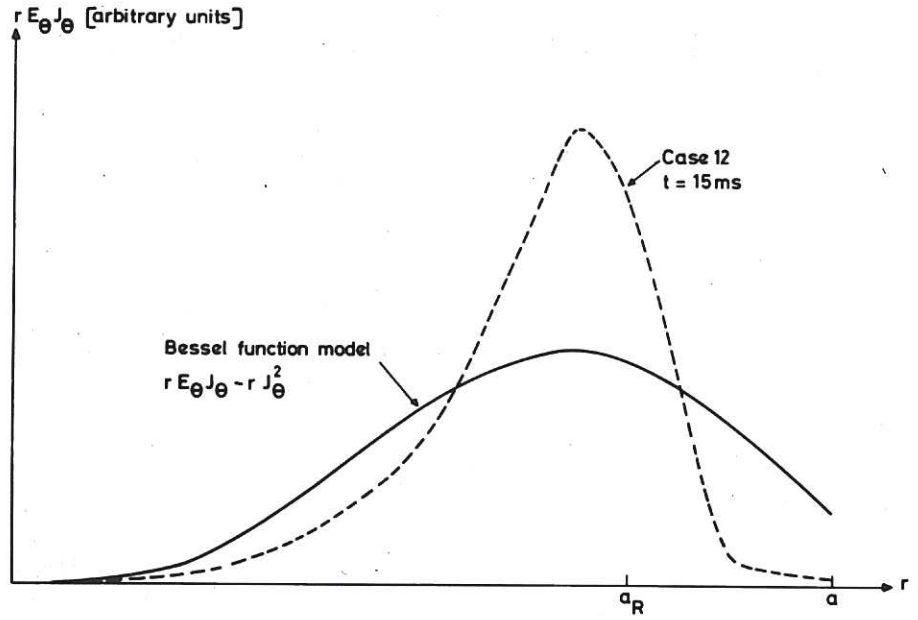

Figure 10 Rate at which B_z energy is transferred to a cylindrical plasma shell of radius r. The full curve is the initial rate obtained for the Bessel function model while the dashed curve shows the rate of B_z energy transfer from a hot central region and a cooler outside region. The dashed curve corresponds to case 12 (Table II) at t = 15 msec. The scaling is arbitrary.

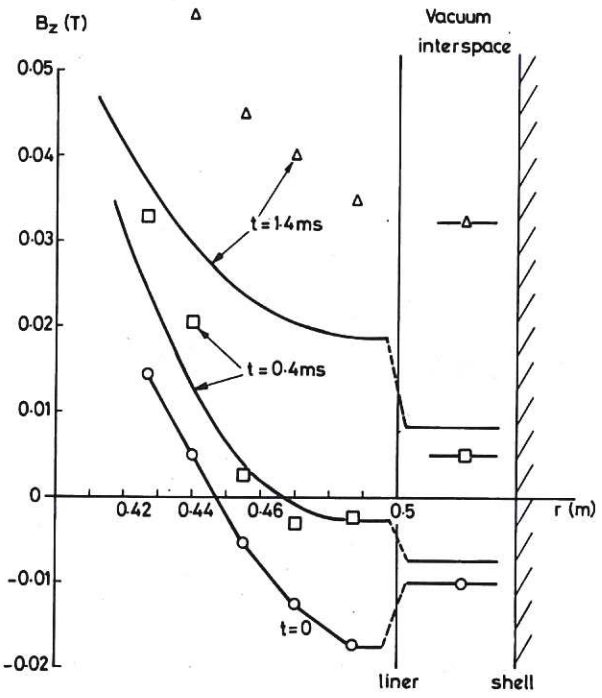

Figure 11 Disappearance of the reversed B_z field in ZETA. The calculated values (case 12 in Table II) are drawn as full curves against the experimental points.

CLM-P484

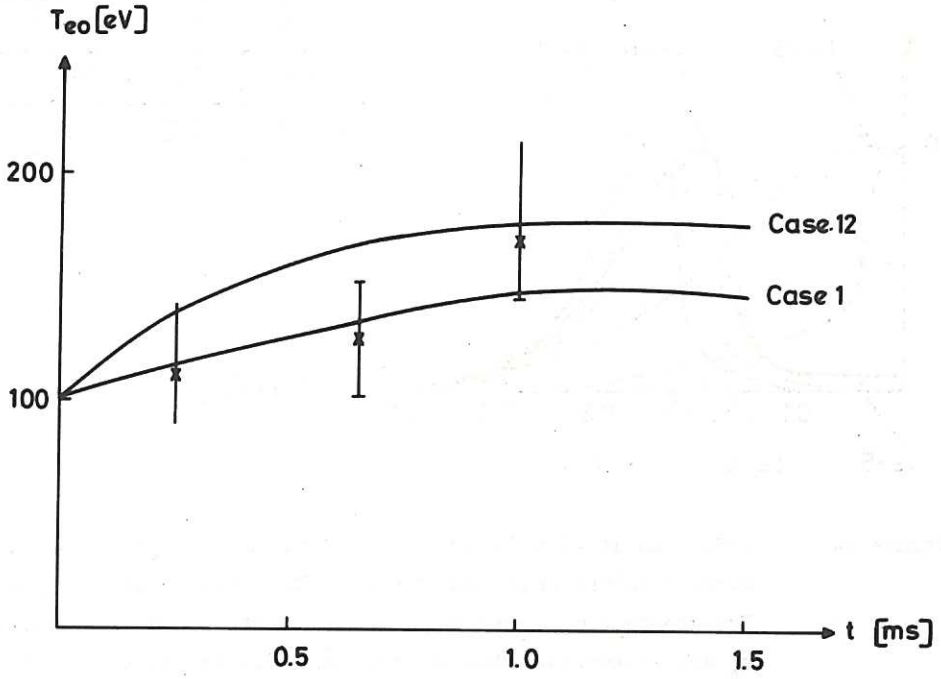

Figure 12 ZETA: Calculated increase in axial electron temperature $T_{eo} = T_e(r = 0)$ for cases 1 and 12 (Table II). The experimental points and error bars are taken from [12].

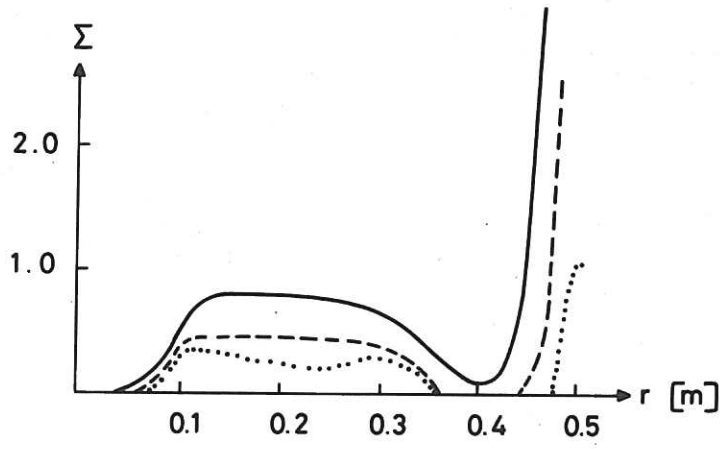

Figure 13 ZETA: Radial variation for the Suydam parameter Σ (equation 25) for case 7 (Table II). Dotted curve t = 0.5 msec. Dashed curve t = 1.0 msec. Full curve t = 1.5 msec.

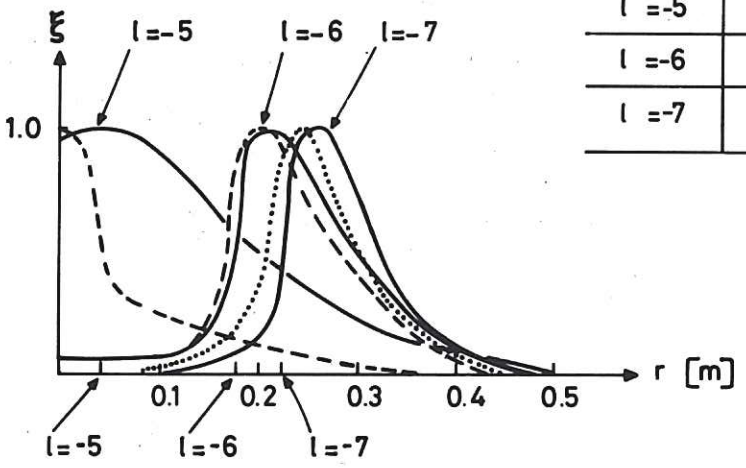

τ [μs]	0.5ms	1 ms	1.5ms
l =-5	0	22	9.9
l =-6	39	29	20
l =-7	410	208	122

Figure 14 ZETA: Radial eigenfunctions for three m = 1 Suydam unstable modes obtained from case 7 (Table II). Legend as in Figure 13. The growth times and the positions of the singular surfaces r_s are indicated. Notice the expansion of the $\ell = -5$ radial eigenfunction which is stable at t = 0.5 msec. The increase in width is associated with the growth of Σ shown in Figure 13.

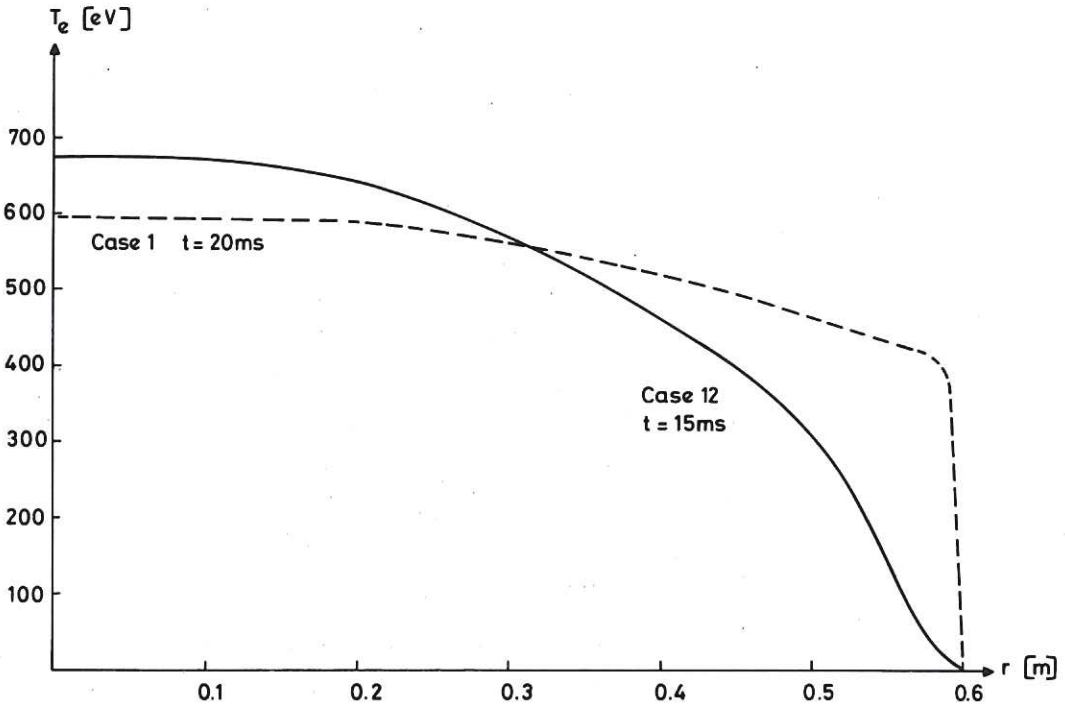

Figure 15 RFX: Electron temperature profiles for cases 1 and 12 (Table II). The ion temperature profile for case 1 (not shown) is much less steep in the outside region.

CLM-P 484

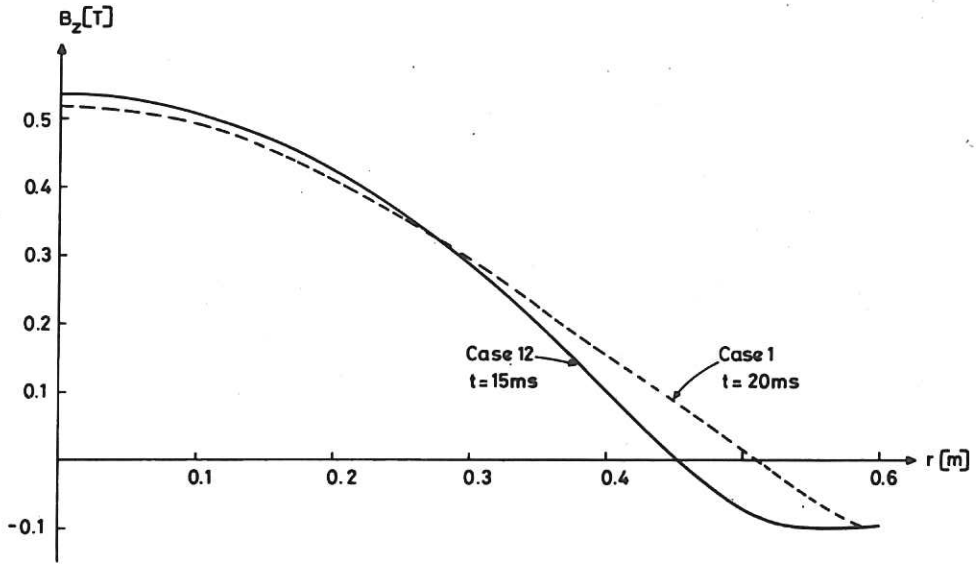

Figure 16 RFX: The difference between the purely classical case 1 and the highly anomalous case 12 is emphasized by the resulting B_z profiles. In case 12 more energy has been transferred from the B_z field to the plasma.

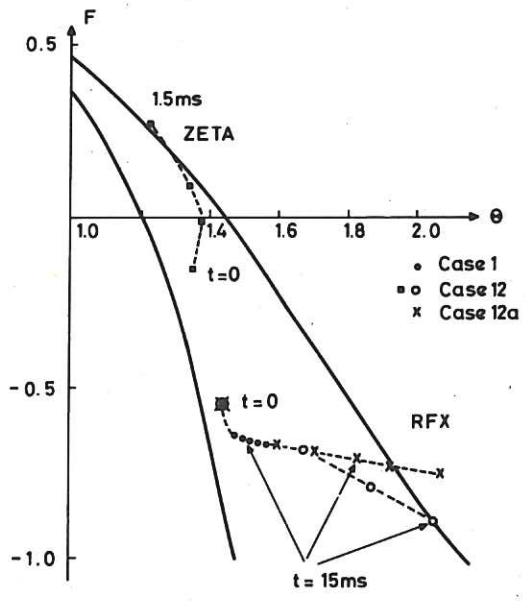

Figure 17 Pinch parameter Θ against field reversal ratio F for ZETA (case 12) and RFX (cases 1,12 and 12a). Case 12a is like case 12, but has $\dot{I}_z/I_z = 0.6\ \dot{\psi}_+/\psi_+$. The increase in β_o leads to a decrease (ZETA) or increase (RFX) in Θ as shown in Figure 3(b). Support of the reversed field (RFX) via programming (equation 40) maintains F and further control of I_z (case 12a) prolongs the stable lifetime. The time spacing between points is 0.5 msec for ZETA and 5 msec for RFX.